PHYSICAL REVIEW C VOLUME 19, NUMBER 4 APRIL 1979

Positive-pion photoproduction on ^{12}C near threshold

F. L. Milder, E. C. Booth, and B. Chasan
Department of Physics, Boston University, Boston, Massachusetts 02215

A.M. Bernstein, J. Comuzzi, and G. Franklin
Physics Department and Laboratory for Nuclear Science, Massachusetts Institute of Technology, Cambridge, Massachusetts 02139

A. Nagl
Department of Physics, Catholic University of America, Washington, D. C. 20064

H. Uberall
Catholic University of America, Washington, D. C. 20064
and Naval Research Laboratory, Washington, D. C. 20375
(Received 17 November 1978)

The π^+ photoproduction on ^{12}C has been measured relative to the proton from 0–20 MeV above threshold. Total cross sections from 0–12 MeV, summed over states in ^{12}B have been extracted with accuracies between 5% and 8% relative to the proton photoproduction cross section. Distorted wave impulse approximation calculations have been performed and show good agreement with the data. The yield from 0–3 MeV above threshold is well described by a one parameter fit for the ground state cross section using only the $\vec{\sigma}\cdot\vec{\epsilon}$ term of the Hamiltonian.

[NUCLEAR REACTIONS $^{12}C(\gamma,\pi^+)^{12}B$, bremsstrahlung endpoint energies to 175 MeV, deduced $\sigma(E)$; calculated $\sigma(E)$, DWIA.]

I. INTRODUCTION

Recent studies of pion photoproduction near threshold have elucidated its threefold nature as a tool of nuclear physics.[1–7] It is a probe of nuclear structure; it tests our understanding of nuclear reaction mechanics; and it is sensitive to the pion-nucleus interaction, most often described by a pion-nucleus optical potential. Given known elementary production amplitudes and a good description of the reaction mechanism, the reaction $A(\gamma,\pi)B$ is an excellent complement to pion scattering and pionic atom experiments. It provides new information on the pion-nucleus optical potential by extending scattering measurements to energies where magnetic analysis is limited by the meson lifetime. Moreover, it provides a continuous transition in momentum transfer from scattering experiments to pionic atoms and is not limited by the cascade of particular pionic orbitals. The nuclear structure information is found in the transition operator matrix elements, which are folded together with production amplitudes and the pion wave functions to obtain the theoretical photoproduction cross section.

The positive pion photoproduction yield on ^{12}C was measured from threshold to 20 MeV excitation in ^{12}B. The yields were obtained with a bremsstrahlung beam and subsequently unfolded to obtain the total cross sections. The results are compared with a theoretical calculation based on the impulse approximation. The calculation is by the method described in Refs. 8–10 and is reviewed here for the specific application to $^{12}C(\gamma,\pi^+)^{12}B$. The inputs to the theory are the elementary production amplitudes, the pion-nucleus optical potential, and a Helm model description of the nuclear matrix elements taken from inelastic electron scattering. The calculation results exhibit very good agreement with the data. A dependence on nucleon-nucleon correlations is demonstrated in that the results depend on the $\rho^2(r)$ terms of the optical potential. The sensitivity of pion-nucleus reactions to these correlations is of considerable theoretical and experimental interest and has been cited in several publications.[11–14]

II. THE EXPERIMENT

The $^{12}C(\gamma,\pi^+)^{12}B$ experiment was performed at the MIT Bates Linear Accelerator. The experimental geometry is shown in Fig. 1. Bremsstrahlung photons were obtained by passing the electron beam through the aluminum of the vacuum end window (0.0033 radiation lengths) and through a beryllium oxide beam viewing screen (0.0017 radiation lengths). The electron beam was typically run with a 3 mA peak current, 1 kHz repetition rate, 2 μsec pulse width and momentum bite $\Delta p/p = 1\times10^{-3}$. The photon beam was monitored with a Wilson quanta-

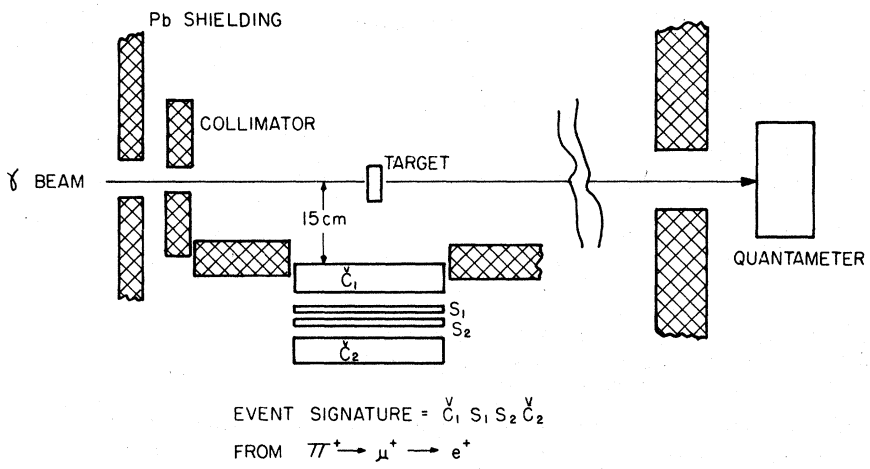

FIG. 1. The experimental geometry. S_1 and S_2 are plastic scintillators. $\check{C}_1$ and $\check{C}_2$ are plastic Cherenkov detectors. The event signature is $\check{C}_1 S_1 S_2 \check{C}_2$ after the beam burst.

meter and corrected for beam burst variations by the "leaky capacitor" method.[15]

The ^{12}C photoproduction yields were measured relative to hydrogen by choosing targets of natural carbon (graphite) and CH_2 (polyethelene). Since the photoproduction cross section on hydrogen is known, many of the possible systematic errors associated with an absolute measurement were eliminated by making a relative measurement. The data were obtained on two separate occasions with different photon beam diameters and target geometries. For data set I, the carbon target was 6.8 cm in diameter and 5.67 gm/cm^2 thick. The CH_2 target dimensions were 7.2 cm by 2.85 gm/cm^2. The photon beam was collimated to a 4 cm beam spot on target. Data set II was taken with C and CH_2 target dimensions of 6.8 cm by 12.07 gm/cm^2 and 7.2 cm by 8.67 gm/cm^2, respectively, and a photon beam spot of 2 cm. For purposes of matching the detector efficiency for the two targets, a 0.6 cm thick aluminum absorber was placed around the CH_2 target for the first data set. (See Data Analysis, Sec. III.)

The photopions were detected via their decay chain $\pi^+ \to \mu^+ \to e^+$. The relativistic positrons were identified by a fourfold coincidence of two 15 cm $\times$ 15 cm plastic Cherenkov counters 3.8 cm thick and two similar plastic scintillators 0.16 cm thick. The detectors were placed at a distance of 15 cm from the target center. Since the positrons are the product of muon decay, they exhibit the characteristic muon mean lifetime of 2.2 μsec. This fact was used to advantage in two ways. It allowed the positrons to be counted between beam bursts when background counts were at a minimum, and it allowed the long lived background to be counted after the muons had decayed (See Data Analysis, Sec. III, Data Set II.) The phototubes were gated off during the beam burst in order to eliminate residual saturation from the enormous photon flux during the burst.

A block diagram of the electronics is shown in Fig. 2. The data were taken in an event-by-event mode with all pulse height and timing information retained for each event.

III. DATA ANALYSIS AND RESULTS

A preliminary evaluation of the experimental results has been reported by Milder *et. al.*[16] The numbers presented here supersede those of Ref. 16, which contained a computational error.

The yield of photopions per nucleus from a bremsstrahlung beam is given by

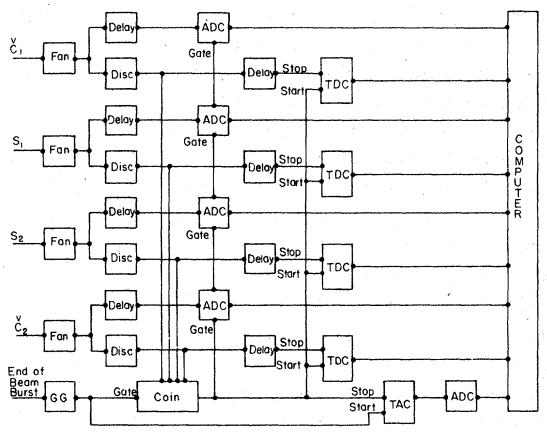

FIG. 2. The electronics used for the event-by-event acquisition of the (γ, π^+) data. All pulse height and timing information is retained for off-line analysis. GG: Gate generator; ADC: analog to digital converter; TDC: time to digital converter; COIN: fourfold coincidence; DISC: discriminator; S_1, S_2, $\check{C}_1$, $\check{C}_2$: arriving signals; FAN: linear fanout. The time to amplitude converter (TAC) records the elapsed time from the end of the beam burst to an event signature.

$$Y(E_0) = \int_{E_T}^{E_0} \sigma(E)\Phi(E, E_0)dE\,, \qquad (1)$$

where σ is the photoproduction cross section, Φ is the bremsstrahlung flux for an incident electron energy E_0, and E_T is the photoproduction threshold. The number of detected events is the yield times $\varepsilon\Omega/4\pi$, where Ω is the detector solid angle and ε is the detector efficiency. Data were taken for 30 bremsstrahlung endpoint energies from 150 MeV to 175 MeV. At each energy several measurements of the yields for both the CH_2 target and the C target were obtained. The statistical error was typically (2–5)%. The data were subsequently analyzed off line and the following corrections were applied (see Table I):

(1) The photopion yields and the quantameter values were corrected for photon flux attenuation in the target.

(2) The pion yields were corrected for electronics deadtime and accidental coincidences. The accidentals arise almost entirely from a true threefold event in random coincidence with the fourth detector.

(3) Using the experimental yields from the graphite target, the relatively small yields of the carbon in the CH_2 were subtracted to produce the hydrogen yields.

(4) Room background and true fourfold coincidences from nonmesic sources were subtracted from the observed yields. This was done with different methods for the two data runs. For data set I, several below threshold points at different energies were taken on both targets. These yields are nomesic in nature and this background was assumed to be constant over the energy range in which the data were taken. The averaged below-threshold yield for each target was subtracted from the data points above threshold. The development of the more sophisticated electronics shown in Fig. 2 permitted the background for the data in set II to be subtracted in a different manner, testing the results obtained in data set I. The recorded information included the elapsed time (t) from the end of the beam burst until the arrival of each event out to 60 μsec. Histograms of this data were fit with the form

$$Ae^{-t/\tau} + B,$$

where τ is the muon lifetime.

The constant term (B) was assumed to be the nonmesic background and should be the only source of counts below threshold. When fitted with the above form, the below-threshold yields were consistent with zero meson production, which justified the method of background subtraction employed in the analysis of data set I.

(5) Natural carbon (in the graphite and the CH_2) consists of 99% ^{12}C and 1% ^{13}C. The $^{12}C(\gamma, \pi^+)^{12}B$ reaction to the ^{12}B ground or first excited state deposits a neutron in the $p_{1/2}$ orbital. In the reaction $^{13}C(\gamma, \pi^+)^{13}B$, this orbital already has one neutron in it. The threshold energies and logft values for β^- decay are nearly identical for these two isotopes, indicating that the $\vec{\sigma} \cdot \vec{\varepsilon}$ matrix elements for the two cases are similar. Therefore, one expects the cross section on ^{13}C to be down from ^{12}C by a factor on the order of 2. Reactions leaving neutrons in other orbitals should be of the same order for ^{12}C and ^{13}C. A correction for the ^{13}C content in natural carbon is thus expected to be (0.5–1.0)%. There exist no experimental data for $^{13}C(\gamma, \pi^+)^{13}B$. We have chosen to ignore the yield due to the ^{13}C impurity. Our ^{12}C cross section is hence an upper bound in error by perhaps (0.5–1.0)% from the true value, other effects being ignored.

TABLE I. Sample comparison of corrections to the raw CH_2 data at 2 MeV and 12 MeV above threshold for data set I. The numbers are typical.

Correction	% at $\Delta E = 2$ MeV	% at $\Delta E = 12$ MeV
Photon flux attenuation	2.7	2.7
Deadtime plus accidentals	0.2[c]	0.3[c]
C contribution to $CH_2(\gamma, \pi^+)$	0.0 (below C threshold)	2.0
Nonmesic background	19.2[b]	0.2[b]
Solid angle[a]	0.2	0.2
Pion end loss[a]	0.2	4.7
Detection efficiency[a] (positron absorption)	2 ± 4	2 ± 4

[a] Correction of CH_2 target relative to the C target.

[b] The nonmesic background for the CH_2 target is negligible. The background for the C target is included here for relative information.

[c] This correction was larger for the carbon target but was generally < 1%.

(6) The efficiency for pion detection ε and the detector average solid angle Ω change as a function of target material, target geometry, beam energy, and discriminator settings, although a large part of these variations cancel in taking a relative measurement. The effective solid angle change with different target geometries was calculated and the appropriate corrections made. A decrease in efficiency with increasing energy was caused by photopions escaping from the ends of the target. No pions were lost through the sides of the target. The pion endloss was taken into account with a model based on pion range-energy formulas. In the model, the near-threshold pion production was taken to be isotropic and the cross section was assumed linear with the energy above threshold. Any pion with sufficient range to exit from the target was considered lost. The number of such pions was calculated by folding together the cross section, the bremsstrahlung flux, and the target geometry. Since this correction was small overall, the model was sufficiently accurate (see Table I). These corrections were confirmed by a Monte Carlo calculation supplied by Van Oystaeyen.[17]

The most important possible change in detector efficiency arose from the difference of target densities, which affected the scattering and annihilation of the exiting positrons in the target. For data set I, 0.6 cm of aluminum was placed between the target and the detectors for the CH_2 target. The energy loss and attenuation of the exiting positrons and thus the pion detection efficiency was calculated to be equivalent for the C target and for the system of the CH_2 target with the aluminum absorber. Also, efficiencies were measured by comparing the ratio of fourfold coincidences to threefold coincidences of the first three detectors. In effect, this measured the fraction of positrons exiting the target with enough energy to be detected by the fourth detector. This measurement agreed with our calculations in indicating that the detection efficiency was matched for the two tar-

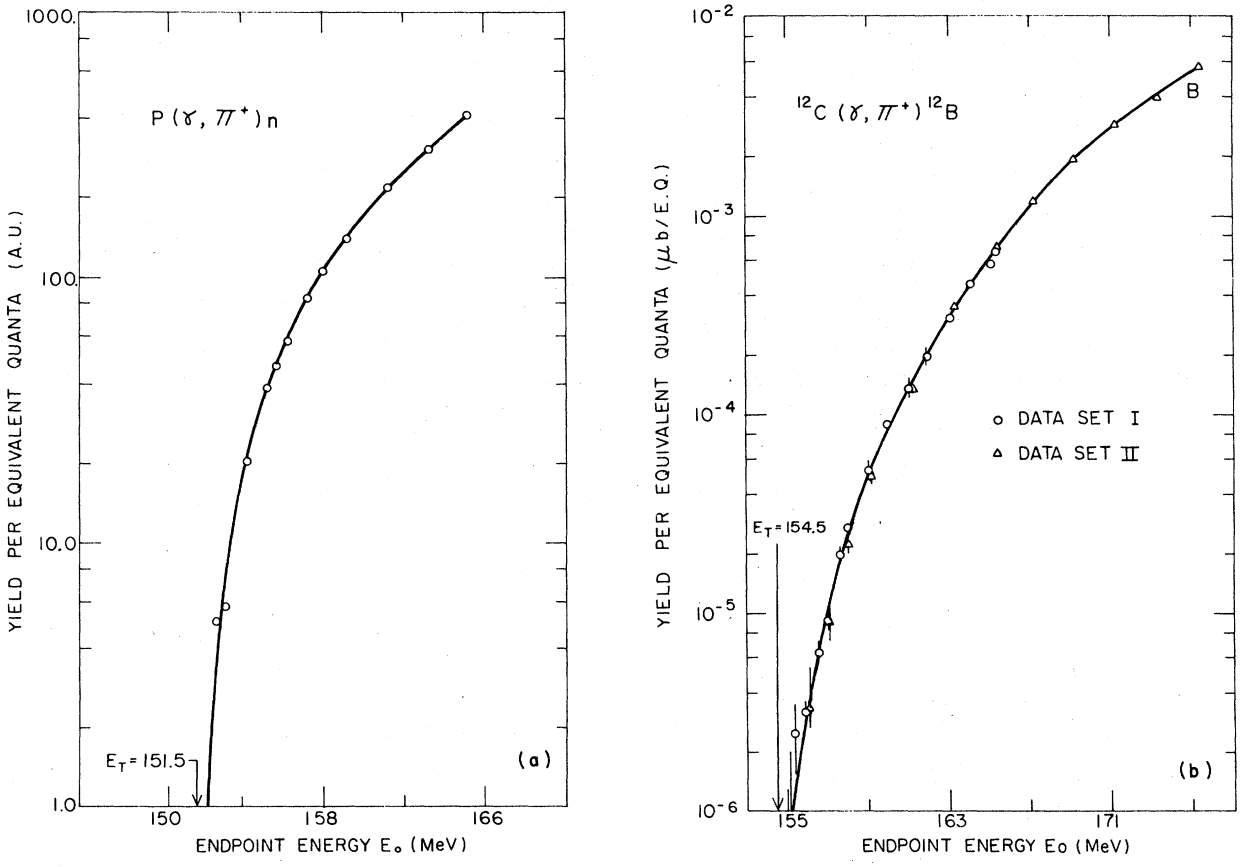

FIG. 3. (a) Experimental yields per equivalent quanta for $p(\gamma,\pi^+)n$ and fit generated from $\sigma_H = 201(p/k)\ (1-0.0063\omega)$. The fit provides the absolute normalization for the experiment. (b) Experimental yields per equivalent quanta for $^{12}C(\gamma,\pi^+)\ ^{12}B$. The solid curve is obtained by folding the bremsstrahlung spectrum with the total summed cross section shown in Fig. 4.

gets. For data set II, no aluminum absorber was used and the yields were corrected according to the calculated efficiencies. The six corrections are given for two sample endpoint energies in Table I. It is useful to define a yield which can be directly compared for different nuclei. The yield per equivalent quanta is defined as

$$\frac{Y(E_0)}{\mathrm{E.Q.}} = \frac{Y(E_0)}{(1/E_0)\int_0^{E_0}\Phi(E,E_0)EdE}\,. \tag{2}$$

This definition allows comparison of data taken with different thickness bremsstrahlung radiators. The quantameter charge is proportional to $\int_0^{E_0}\Phi(E,E_0)EdE$. Figures 3a and 3b show the measured yields per equivalent quanta as a function of bremsstrahlung endpoint energy for hydrogen and carbon. Also shown are various fits to the data described below.

A measurement of the hydrogen yield is used to determine both the absolute normalization of the experiment (given by $\varepsilon\Omega/4\pi$) and the absolute energy scale. Using Eqs. (1) and (2), a two parameter fit to the hydrogen yield data is generated by integrating the known hydrogen cross section with the bremsstrahlung flux. The solid line of Fig. 3(a) is this generated yield. The two parameter cross section is

$$\sigma_H = a_H\frac{p}{k}(1-b_H\omega)\,, \tag{3}$$

where p is the pion momentum, k is the incoming photon momentum, ω is the energy above threshold and σ is in μb. The experimental values[18] are $a_H = 201$ μb and $b_H = 0.0063$ MeV^{-1}. All values are in the center-of-momentum frame. The bremsstrahlung flux is given by a Bethe-Heitler spectrum corrected near the endpoint.[19] The fitting parameters are adjusted to obtain the normalization and the absolute energy scale. The estimated errors are 1% in the normalization and 50 KeV, resulting in a 50 KeV uncertainty in the energy of the carbon data points. The slope of the energy scale is well known from the electron beam optics of the accelerator. As can be seen in figure 3(a), this procedure provides an excellent fit to the hydrogen data.

The carbon yield shown in figure 3(b) was analyzed in two different ways, the first being a fit to the first 3 MeV to obtain the ground state cross section and the second being a polynomial fit to the entire energy range which determines the total cross section summed over the ground and excited states up to 20 MeV excitation in ^{12}B. The $\vec{\sigma}\cdot\vec{\varepsilon}$ term of the transition operator is expected to be dominant near threshold (Sec. IV, Theory) so the cross section for the transition to the ^{12}B ground state can be approximated[6] by

$$\sigma_{^{12}\mathrm{C}} = \frac{ap}{k}S\,, \tag{4}$$

where a is a constant and S is a factor that takes into account the Coulomb distortion of the outgoing pion wave.[20] This form of σ ignores the energy dependences of the fundamental nucleon amplitude, the nuclear matrix element, and the pion-nuclear optical potential. The full distorted-wave impulse approximation (DWIA) calculations (Table III) were fit to within a few percent by

$$\sigma_{^{12}\mathrm{C}} = \frac{ap}{k}S(1-0.01\omega)\,, \tag{5}$$

so expression (4) is adequate for $\omega < 3$ MeV.

To a good approximation, the carbon yields for the first 3 MeV are completely dominated by the ground state cross section. Despite the fact that there are four states in ^{12}B with excitation energies lower than 3 MeV, the bremsstrahlung shape weights the ground state heavily in the final yields. Fitting the first 3 MeV with yields generated from Eqs. (1), (2), and (4), the cross section for $^{12}\mathrm{C}(\gamma,\pi^+)^{12}\mathrm{B}_{\mathrm{g.s.}}$ was found to be

$$\sigma_{^{12}\mathrm{C}} = (0.076\pm0.005)a_H\frac{p}{k}S\,,$$

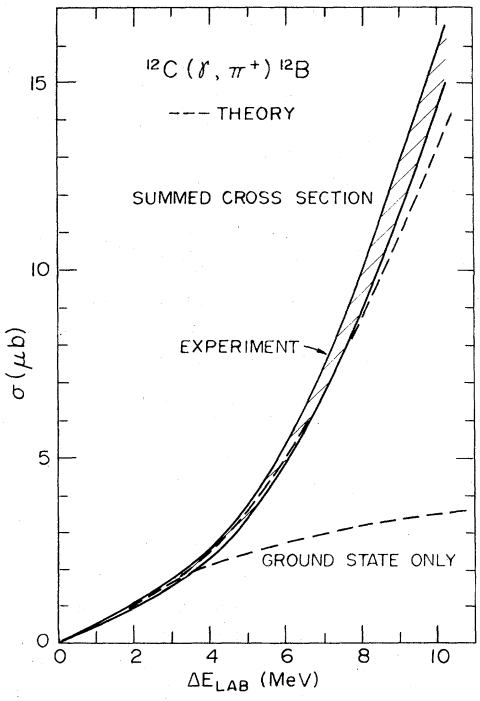

FIG. 4. Unfolded total summed $^{12}\mathrm{C}(\gamma,\pi^+)^{12}\mathrm{B}$ cross section from a fit to the measured yields. The width of the line represents the total estimated error. The upper dashed line is the theoretical summed cross section from Table II. Also shown as a dashed line is the ground state calculation $\sigma^{\mathrm{I}}_{\mathrm{DWIA}}$ from Table III.

which gives $\sigma_{g.s.} = 1.10 \pm 0.07$ μb at $\Delta E_{Lab} = 2$ MeV.

The total cross-section was obtained in the following manner. The raw deuterium data were corrected and normalized to the hydrogen data, which determined the energy calibration and the counter efficiency. It was assumed that the cross section can be represented by a polynomial of arbitrary order in powers of $(E_0 - E_T)$. This polynomial was used to generate the yield $Y(E_0)$ using Eqs. (1) and (2), and the yield was fitted to the observed yield over the entire range of E_0 values to determine the best values of the coefficients in the polynomial. The best fit was obtained with a fifth order polynomial ($\chi^2/\nu = 2.5$). The fitted cross section is given in Fig. 4 along with the calculated cross section which was computed as discussed in Sec. IV. The shaded region represents the statistical error on the fitted cross section. Also shown in Fig. 4 is the calculated cross section for the ground state transition only.

IV. THEORY

The theoretical cross sections were obtained using essentially the formalism outlined in Ref. 9, the major difference consisting in the use of the improved optical potential described below. The differential cross section in the pion-nucleus center-of-momentum (c.m.) system (which in practice coincides with the lab system), averaged over photon polarizations, and averaged over the final and initial spin projections M_f, M_i, respectively, is

$$\frac{d\sigma}{d\Omega} = \frac{p}{k}\,\frac{M_A M_{A'}}{W_i W_f}\,\frac{1}{2J_i+1}\sum_{M_i M_f}\sum_{\lambda}\left|T_{fi}^{(\gamma\pi)}\right|^2, \tag{6}$$

where p and k are the pion and photon momenta, M_A and $M_{A'}$ the initial and final nuclear masses, W_i and W_f the initial and final total energies, and λ the photon polarization index.

In the impulse approximation, the nuclear T matrix can be written

$$T_{fi}(\vec{p},\vec{k}) = \sum_n \int d^3 p_i\, t_f^n(\vec{p},\vec{k},\vec{p}_i)\rho_{fi}{}^n(\vec{p}_i - \vec{q},\vec{p}_i), \tag{7}$$

where $\vec{q} = \vec{k} - \vec{p}$. It consists of an integral over the initial nucleon momentum p_i, the product between t_f^n, the photoproduction amplitudes on a free nucleon, and the nuclear transition densities ρ_{fi}^n. In Eq. (7), it is implied that the total photoproduction operator t_f has been divided into parts having the same nucleon operators O^n as factors, i.e.,

$$t_f = \sum_n t_f^n O^n, \tag{8}$$

where

$$O^1 = \vec{\sigma}\tau \text{ and } O^2 = \tau, \tag{9}$$

with τ the appropriate isospin operator, and that the quantities ρ_{fi}^n are the nuclear matrix elements of the operators O^n. The amplitudes t_f^n are functions of the initial nucleon momentum $\vec{p}_i$, so it appears necessary to carry out the integration in Eq. (7). However, it may be seen that due to the approximate symmetry of ρ_{fi}^n about the value of the argument

$$\vec{p}_i = \tfrac{1}{2}(\vec{p} - \vec{k}) = \vec{p}_0, \tag{10}$$

one can take the amplitudes t_f^n out of the integral without introducing a serious error. Moreover in the threshold region, which is of interest here, the terms in t_f^n proportional to $\vec{p}_i$ are small, so that one may use a factoring approximation and write, after going to the configuration space, for the T matrix

$$T_{fi}(\vec{p},\vec{k}) = \sum_n t_f^n(-i\vec{\nabla},\vec{k},\vec{p}_0)\int d^3 r \phi_\pi^{(-)*}(\vec{r}) e^{i\vec{k}\cdot\vec{r}}\rho_{fi}^n(\vec{r}), \tag{11}$$

where $\phi_\pi^{(-)}(\vec{r})$ is the distorted pion wave, and where

$$\rho_{fi}^n(\vec{r}) \equiv \left\langle J_f M_f \left| \sum_{j=1}^{A} O_j^n\, \delta(\vec{r} - \vec{r}_j) \right| J_i M_i \right\rangle \tag{12}$$

are the nuclear transition densities corresponding to the operators of Eq. (9). These densities contain all the nuclear physics of the problem.

Using Eq. (10) one obtains for the free t matrix in the lab system

$$t_f(\vec{p},\vec{k}) = i\vec{\sigma}\cdot\vec{\varepsilon}F_1 + \vec{\sigma}\cdot\vec{p}\vec{\sigma}\cdot(\vec{k}\times\vec{\varepsilon})(F_2/pk) + i\vec{\sigma}\cdot\vec{k}\vec{p}\cdot\vec{\varepsilon}(F_3/pk) + i\vec{\sigma}\cdot\vec{p}\vec{p}\cdot\vec{\varepsilon}(F_4/p^2) \tag{13}$$

(ε = photon polarization vector), which has the same form as the free t matrix in the pion-nucleon c.m. system, except that now all quantities are expressed in the lab system. The coefficients F_i are obtained by using the elementary amplitudes of Ref. 21 which are given in the photon-nucleon c.m. system, and transforming them to the laboratory system.[10] This is accomplished by using the invariant amplitudes of the relativistic form of the transition operator as an intermediate step. To approximately account for the off-shell form in which the elementary t matrix is needed in Eq. (7) we proceed as outlined in Ref. 9. The above procedure, when used to calculate the hydrogen photoproduction cross section near threshold, agrees with the measured value of b_H [see Eq. (3)] but gives a value for $a_H = 215$ μb. Since the experimental cross sections are normalized by the value of a_H, we have scaled down our theoretical ^{12}C cross sections by 7% in order to directly compare them with the experiment.

In the region of excitation energies covered by this experiment, a considerable number of final

nuclear states had to be included in the calculation. The transition densities between the ground state of ^{12}C and these levels were obtained by Helm model fits to electroexcitation data of the corresponding analog states in ^{12}C. A list of these levels, and of the fitted Helm model parameters, appears in Ref. 22. For the present purpose, these parameter values are used, except those of the levels labeled No. 1–4 which were refitted with the additional use of more recently available data.[23] We also disregarded the contributions of levels No. 6 and 12 which were observed in electroexcitation of ^{12}C, but have no apparent counterparts[24] in ^{12}B so that their previous assignment[25] of $T=1$ is questionable.

Helm parameters of the giant dipole resonance (which contributes at energies above 5.6 MeV from threshold in ^{12}B) had been obtained[22] from a fit to the experimental form factor integrated[25] over 21–26 MeV excitation in ^{12}C. In order to approximate the continuous nature of this excitation range, we divided the region into five 1 MeV bins whose contributions enter successively into the calculation as the excitation energy is raised.

Wave functions for $\pi^{\pm}$ mesons are calculated by solving the Klein-Gordon equation using the strong-interaction optical potential

$$V_{\rm st}=-\frac{2\pi}{E_\pi}\left\{\left(1+\frac{E_\pi}{m}\right)\left[b_0\rho(r)\pm b_1(\rho_n-\rho_p)\right]+\frac{E_\pi}{2m}\nabla c'(r)+B\left(1+\frac{E_\pi}{2m}\right)\rho^2(r)-\left(1+\frac{E_\pi}{m}\right)^{-1}\vec{\nabla}\cdot\frac{c'(r)}{1+(4\pi/3)\xi c'(r)}\vec{\nabla}-C\left(1+\frac{E_\pi}{2m}\right)^{-1}\vec{\nabla}\cdot\rho^2(r)\vec{\nabla}\right\} \quad (14a)$$

(in addition to the Coulomb potential), where

$$c'(r)=c_0\rho(r)+c_1[\rho_n(r)-\rho_p(r)]\,, \quad (14b)$$

$\rho(r)$ being the sum of proton (ρ_p) and neutron (ρ_n) densities. Here E_π = total pion energy and m = nucleon mass. We shall make the usual approximation $\rho_n-\rho_p=[(N-Z)/A]\rho$.

The complex values of the optical potential parameters b_0, b_1, c_0, and c_1 were obtained in the standard way from free pion-nucleon scattering phase shifts, which are functions of energy, and for which we used recent results of Rowe *et al.*,[26] except that Re b_0 was changed, using pionic atom data,[27] to the value $-0.03\mu^{-1}$ (μ = pion mass). The values of the coefficients of the pair terms B and C were taken as follows: Im $B=0.042\ \mu^{-4}$ and Im $C=0.076\ \mu^{-6}$ using the pionic atom data.[28] Re B and Re C were taken equal and opposite to these values.[28] The Lorentz-Lorenz parameter ξ was chosen equal to unity[29] which is consistent with pionic atom data.[28]

V. DISCUSSION

Table II summarizes a comparison of the experimental unfolded cross sections with our theoretical DWIA calculation. The cross sections in column 2 are the experimental total ^{12}C$(\gamma,\pi^+)^{12}$B cross sections summed over states in ^{12}B including all estimated errors. Column 3 is the calculation as given by Eq. (6) for that same cross section using our best estimates for the pion-nucleus optical potential of Eq. (14). The values of column 3 are also plotted as a dashed line in Fig. 4. The overall agreement with the experiment for the chosen optical potential parameters is seen to be quite good, although the theoretical cross sections at the higher energies are slightly below the experimental values. The magnitude of this discrepancy is only 12% at 10 MeV and is an indication that the theory does not include enough excited state strength. Figure 5 displays the components of the total DWIA cross section as a function of energy above threshold. The states are labeled as in Ref. 22. Since the nuclear wave function information for the giant dipole resonance (GDR) is relatively less accurate (the Helm parameters are from integrated cross sections and the dipole's continuous nature has been approximated), and since the GDR contributes a large fraction of the total cross section at higher energies, the missing strength could well be in the GDR. Another possibility for the missing cross section could be contributions from quasifree photoproduction since the neutron separation energy for ^{12}B is only 3.4 MeV.

Our experiment is not able to discriminate among these and other alternatives in the 10 MeV region. Recently, photoproduction differential cross sections at 90° were obtained with momentum analyzed[30] outgoing pions.

These experiments are better able to obtain the meson yields for individual levels and should help decide where the unaccounted for cross section resides.

Table III compares DWIA calculations of the

TABLE II. Comparison of the total summed ^{12}C cross section with DWIA theoretical calculation at several photon energies above threshold.

$\Delta E_{\rm Lab}$	$\sigma_{\rm exp}$ (μb)	$\sigma^I_{\rm DWIA}$ (μb)
2	1.02 ± 0.08	1.23
4	2.33 ± 0.15	2.47
6	5.07 ± 0.24	5.04
8	9.42 ± 0.48	8.75
10	14.99 ± 0.69	13.13

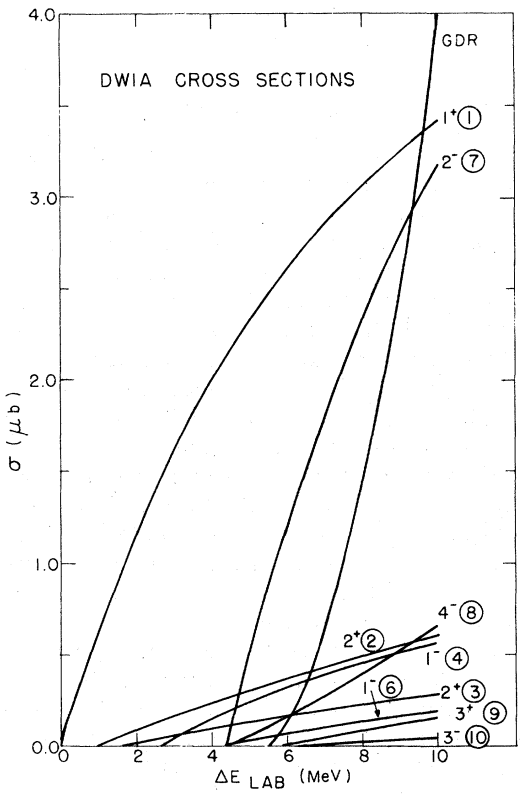

FIG. 5. Calculated DWIA cross sections for $^{12}C(\gamma,\pi^+)^{12}B$ to individual levels in ^{12}B as a function of energy above threshold. The states are labeled according to Ref. 21.

ground state cross section and indicates their sensitivity to the choice of optical model parameters.

Column 2 presents the DWIA ground state cross section with the best choice of coefficients B and C for the pair terms as given in the theory section. Column 3 is the same calculation only with $\mathrm{Re}\,B = \mathrm{Re}\,C = 0$. Column 4 has $B = C = 0$. It can be seen from comparisons of columns 3 and 4 with column 2, that the photoproduction near threshold is indeed sensitive to nucleon-nucleon correlations through the pair terms of the optical potential.

TABLE III. Comparison of the ground state DWIA calculations for three sets of optical potential pair parameters. The experimental result at $\Delta E_{\mathrm{Lab}} = 2$ MeV is $\sigma_{g.s.} = 1.10 \pm 0.07$ μb. $\sigma^{\mathrm{I}}_{\mathrm{DWIA}}$ is the cross section given by the best choice of parameters from pionic atom and pion scattering data.

ΔE_{Lab}	$\sigma^{\mathrm{I}}_{\mathrm{DWIA}}$ [a]	$\sigma^{\mathrm{II}}_{\mathrm{DWIA}}$ [b]	$\sigma^{\mathrm{III}}_{\mathrm{DWIA}}$ [c]
2	1.13	1.34	1.36
4	2.01	2.36	2.42
6	2.62	3.06	3.17
8	3.07	3.59	3.74
10	3.42	3.99	4.18

[a] $\mathrm{Re}B = -\mathrm{Im}B$; $\mathrm{Re}C = -\mathrm{Im}C$.
[b] $\mathrm{Re}B = 0$; $\mathrm{Re}C = 0$.
[c] $\mathrm{Re}B = \mathrm{Im}B = 0$; $\mathrm{Re}C = \mathrm{Im}C = 0$.

The experimental ground state cross section at $\Delta E_{\mathrm{lab}} = 2$ MeV obtained from the one parameter fit was $\sigma_{g.s.} = 1.10 \pm 0.07$ μb, in good agreement with the calculation in column 2 of Table III. This experimental result is expected to be more accurate than the value of 1.02 ± 0.08 μb given in Table II, which was obtained from the model independent fit to the total summed cross section over the entire energy range.

The dependence of the DWIA cross section on the Lorentz-Lorenz parameter also was tested. For reasonable choices of ξ, the cross section varies only a few percent, so the experiment neither confirms nor disputes the choice of $\xi = 1$.

VI. CONCLUSIONS

The charged pion photoproduction yield was measured relative to the proton for the reaction $^{12}C(\gamma,\pi^+)^{12}B$. The first 3 MeV of yield have been fit to obtain the ground state cross section given by $\sigma_{g.s.} = (0.076 \pm 0.005)\, a_H(p/k)S$. The observed yield up to 20 MeV was unfolded to obtain the total photoproduction cross section summed over all states. The theory, based on a DWIA calculation, is in good agreement with the data. No parameters were adjusted to obtain this agreement. The nuclear transition matrix elements were parametrized by the Helm model using parameters obtained from magnetic electron scattering. The pion optical model parameters were obtained from pionic atom and pion scattering data. There is a good deal of freedom in choosing a particular pion-nucleus optical potential, and our choice of the potential parameters is supported by the agreement with the data. There is a slight discrepancy between theory and experiment for the total cross section at the higher energies. The experimental cross section is slightly greater than the theory at 8 and 10 MeV above threshold. The magnitude of this disagreement is at the 10% level. This is probably due to excluding some excited state strength or to the onset of quasifree photoproduction. Recent photopion experiments with the pions momentum analyzed[30] should prove useful in resolving this discrepancy.

We would like to thank the Massachusetts Institute of Technology Bates Linear Accelerator staff for their support throughout the experiment. We also wish to thank Mr. J. Ertel for his help with the Helm model fits, and Dr. B. L. Roberts for useful discussions and his critical reading of the manuscript. This work was supported in part by the National Science Foundation and in part by the U.S. DOE.

[1]Francis J. Kelly, Lawrence J. McDonald, and H. Überall, Nucl. Phys. A139, 329 (1967).
[2]J. H. Koch and T. W. Donnelly, Nucl. Phys. B64, 478 (1973).
[3]C. Tzara, Nucl. Phys. A256, 381 (1976).
[4]A. M. Bernstein, N. Paras, W. Turchinetz, B. Chasan, and E. C. Booth, Phys. Rev. Lett. 37, 819 (1976).
[5]E. C. Booth, B. Chasan, A. M. Bernstein, P. Bosted, and J. H. Koch, Phys. Lett. 66B, 236 (1977).
[6]G. Audit, A. Bloch, N. deBotton, C. Schuhl, G. Tamas, C. Tzara, J. Deutsch, D. Favart, R. Prieels, and B. Van Oystaeyen, Phys. Rev. C 15, 1415 (1977).
[7]G. Audit, A. Bloch, N. deBotton, J. L. Faure, C. Schuhl, G. Tamas, C. Tzara, E. Vincent, J. Deutsch, D. Favart, R. Prieels, and B. Van Oystaeyen, Phys. Rev. C 16, 1517 (1977).
[8]F. Cannata, B. A. Lamers, C. W. Lucas, A. Nagl, H. Überall, and C. Wentz, Can. J. Phys. 52, 1405 (1974).
[9]A. Nagl and H. Überall, Phys. Lett. 63B, 291 (1976).
[10]A. Nagl, F. Cannata, and H. Überall, Acta Phys. Austriaca 48, 267 (1978).
[11]R. R. Johnson, T. G. Masterson, K. L. Erdman, A. W. Thomas, and R. H. Landau, Nucl. Phys. A296, 444 (1978).
[12]M. A. Moinester, R. L. Burman, R. P. Redwine, M. A. Yates-Williams, D. J. Malbrough, C. W. Darden, R. D. Edge, F. E. Bertrand, T. P. Cleary, E. E. Gross, C. A. Ludemann, M. Blecher, K. Gotow, D. Jenkins, and F. Milder, Phys. Rev. C 18, 2678 (1978).
[13]L. C. Liu, Phys. Rev. C 17, 1787 (1978).
[14]G. E. Brown, B. K. Jennings, and V. Rostokin, The Pion-Nucleus Many Body Problem, LASL Summer Workshop 1977, Report No. LA-6926-C (unpublished), pp. 1–44.
[15]J. L. Block and J. Mahieux, Nucl. Instrum. Methods 58, 93 (1968).
[16]F. L. Milder, E. C. Booth, B. Chasan, A. Bernstein, J. Comuzzi, and G. Franklin, Bull. Am. Phys. Soc. 23, 611 (1978).
[17]B. Van Ostaeyen, private communication.
[18]G. Audit *et al.*, Phys. Rev. C 16, 1517 (1977) and references cited therein.
[19]J. L. Matthews and R. O. Owens, Nucl. Instrum. Methods 91, 37 (1971).
[20]C. Tzara, Nucl. Phys. B18, 246 (1970).
[21]F. A. Berends, A. Donnachie, and D. L. Weaver, Nucl. Phys. B4, 1 (1967).
[22]H. Überall, B. A. Lamers, J. B. Langworthy, and F. J. Kelly, Phys. Rev. C 6, 1911 (1972).
[23]J. B. Flanz *et al.*, Bull. Am. Phys. Soc. 23, 583 (1978); J. B. Flanz and G. A. Peterson, private communication.
[24]F. Ajzenberg-Selove, Nucl. Phys. A248, 1 (1975).
[25]A. Yamaguchi, T. Terasawa, K. Nakahara, and Y. Torizuka, Phys. Rev. C 3, 1750 (1971).
[26]G. Rowe, M. Salomon, and R. Landau, Proceedings of the Seventh International Conference on High Energy Physics and Nuclear Structure, Zurich, 1977 (unpublished).
[27]M. Krell and T. E. O. Ericson, Nucl. Phys. B11, 521 (1969).
[28]J. Hufner, Phys. Rep. 21C, 1 (1975).
[29]M. Ericson and T. E. O. Ericson, Ann. Phys. (N.Y.) 36, 327 (1966).
[30]N. Paras, A. M. Bernstein, K. I. Blomqvist, G. Franklin, M. Pauli, B. Schoch, L. LeRose, K. Min, D. Rowley, P. Stoler, E. J. Winhold, and P. F. Yergin, Proceedings of the International Symposium on Photopion Nuclear Physics, Rensselaer Polytechnic Institute, 1978 (unpublished).